Key Role of Phenylalanine 20 in Cytochrome c_3: Structure, Stability, and Function Studies†

Alain Dolla,‡ Pascal Arnoux,§ Irina Protasevich,|| Vladimir Lobachov,|| Marianne Brugna,‡ Marie Thérèse Giudici-Orticoni,‡ Richard Haser,⊥ Mirjam Czjzek,§ Alexander Makarov,|| and M. Bruschi*,‡

Laboratoire de Bioénergétique et Ingénierie des protéines, UPR 9036 C.N.R.S., Laboratoire d'Architecture et Fonction des Macromolécules Biologiques, UPR 9039 C.N.R.S., Institut de Biologie Structurale et Microbiologie, 31 chemin J. Aiguier, 13402 Marseille, Cedex, 20 France, and Engelhardt Institute of Molecular Biology, Russian Academy of Sciences, Vavilov strasse 32, Moscow 117984, Russia

Received July 6, 1998; Revised Manuscript Received September 28, 1998

ABSTRACT: Aromatic residues in c-type cytochromes might have an important function in the folding and/or electron transferring properties of the molecule. In the tetraheme cytochrome c_3 (M_r 13 000) from *Desulfovibrio vulgaris* Hildenborough, Phe20, is located between heme 1 and heme 3 with its aromatic ring close and almost parallel to the ring plane of heme 1. We replaced this residue by a nonaromatic hydrophobe residue, leucine, and analyzed the effects in terms of functional, structural, and physicochemical properties. While the F20L replacement did not have any strong effects on the heme region stability, a decrease of the thermostability of the whole molecule was observed. In the same way, the four macroscopic redox potentials were affected by the mutation as well as the flexibility of the surface loop around heme 4. The F20L replacement itself and/or this structural modification might be responsible for the loss of the intermolecular cooperativity between F20L cytochrome c_3 molecules.

C-type cytochromes are electron transport proteins acting in most of the respiratory electron chains. Depending on the heme content, several classes of c-type cytochromes can be distinguished. Among them, the Class III, as defined by Ambler (*1*), contains the multiheme c-type cytochromes characterized by a bis-histidinyl coordination type of the heme iron atoms. One of the most studied members of this class is the tetraheme cytochrome c_3 (M_r 13 000) that is found in all sulfate-reducing bacteria belonging to the *Desulfovibrio* genus. This cytochrome is characterized by the presence of four c-type heme groups exhibiting very low oxidoreduction potentials ranging −400 to −165 mV (*2*). These negative values confer to this class of cytochromes an important function in the anaerobic respiration of sulfate (*3*). The three-dimensional structures of five cytochromes c_3 (M_r 13 000) have been solved to date (refs 4, and references therein, and 5) and comparison of these structures revealed that the overall folding was very well conserved, especially in terms of heme core geometry. In contrary, the alignment of 10 sequences of cytochrome c_3 (M_r 13 000) from various species revealed a low sequence identity. Most of the 24 conserved residues are involved in both the heme-binding sites and the iron atom coordination. In addition to these residues, several aromatic residues are conserved, and their location in the three-dimensional structure is almost identical as well. Among them, phenylalanine 20 is the most interesting residue, located between heme 1 and heme 3 (sequential numbering) with the aromatic ring close and almost parallel to ring plane of heme 1. It has been suggested that this residue might be involved in the intramolecular electron transfer within the cytochrome molecule. A hypothetical intramolecular electron-transfer pathway has been proposed from heme 4, the electron entrance gate, to heme 1, the electron transfer being greatly facilitated by several structural features (*6*). The first step of this pathway would be an electron exchange between heme 4 and heme 3, followed by an electron transfer from heme 3 to heme 1. During this last step, phenylalanine 20 might have an important function in facilitating the electron exchange between the two heme groups. Recently, this residue has been replaced by either an isoleucine or a tyrosine residue (*7*). Surprisingly, the authors reported that these replacements had only small effects on the redox potentials of the heme groups and concluded that this residue, namely F20, has no essential role in either electron/electron or electron/proton cooperativity. On the other hand, several mutations of the histidines, sixth axial ligands to the heme iron atom, have been shown to greatly affect either the electron-transfer rate with the redox partner (*8*) or the thermostability of the molecule (*9*).

In this paper, we report the replacement of the phenylalanine 20 of the cytochrome c_3 (M_r 13 000) from *D. vulgaris* Hildenborough by a nonaromatic hydrophobe residue, leucine, and the effects of this replacement on the functional

† This work was supported by the PICS 486 from CNRS and the RFFI-CNRS 98-04-22001 from the Russian Fund of Fundamental Research.

* Corresponding author. Tel: 33 4 91 16 41 44. Fax: 33 4 91 77 95 17. E-mail: bruschi@ibsm.cnrs-mrs.fr.

‡ Laboratoire de Bioénergétique et Ingénierie des protéines.

§ Laboratoire d'Architecture et Fonction des Macromolécules Biologiques.

|| Russian Academy of Sciences.

⊥ Present address: Institut de Biologie et Chimie des Protéines, CNRS, 7 Passage du Vercors, 69367 Lyon Cedex 07, France.

[1] Abbreviations: EDTA, (ethylenediamine)tetraacetic acid; Hepes, N-(2-hydroxyethyl)piperazine-*N*′-2-ethanesulfonic acid.

10.1021/bi981593h CCC: $18.00
Published on Web 12/12/1998

Table 1: Bacterial Strains and DNA Vectors Used

D. desulfuricans G200	Spontaneous Nal^r derivative of *D. desulfuricans* G100A[a]
E. coli TG2	Δ(*lac-pro*) *SupE thi hsdM hsdR RecA* F′(*traD36 proAB*$^+$ *lacZDM15 I*^{q})
M13mpj800	contains the *cyc* gene of *D. vulgaris* Hildenborough on a 640-base pair *Eco*RI−*Hin*dIII insert in M13mp8 (*8*)
pJRD215	IncQ group, broad-host-range cloning vector, Km^{r}Sm^r [a]
pJRC800F20L	contains the mutated F20L *cyc* gene on a 640-base pair *Eco*RI−*Hin*dIII insert in pJRD215 (this study)

[a] See ref 15.

and physicochemical properties as well as on the three-dimensional structure of the molecule.

EXPERIMENTAL PROCEDURES

Strains, Vectors, and Growth Conditions. The bacterial strains and plasmids used in this study are described in Table 1. Growth of *Escherichia coli* strains was carried out in TY medium (*10*) supplemented by the appropriate antibiotic, 0.27 mM ampicillin or 0.17 mM kanamycin, respectively. Large-scale culture of *Desulfovibrio desulfuricans* G200 was in medium C (*11*) supplemented with 0.26 mM kanamycin.

Site-Directed Mutagenesis. Phagemid M13mpj800 served as the source for the *D. vulgaris* Hildenborough cytochrome c_3 (M_r 13 000) gene *cyc* (*8*). The mutagenic oligonucleotide F20L (5′ CCGTGTTTTGAACCACTCCA 3′) was designed to change the TTC codon at nucleotide 277−279 (*12*), encoding F20, into TTG encoding a leucine residue. The mutation was introduced using the Sculptor IVM in vitro mutagenesis kit from Amersham Life Science, based on the method of Eckstein (*13*). The mutation was checked by sequencing with the dideoxy chain termination method (*14*). The replicative form of the M13 DNA, carrying the desired mutation, was digested with both *Eco*RI−*Hin*dIII, and the resulting 640 base pair fragment was transferred to pJRD215 previously cut with the same two enzymes to give pJRC800F20L. This plasmid was then transferred to *D. desulfuricans* G200 as previously described (*15*).

Purification of the F20L Cytochrome c_3 Expressed in D. desulfuricans G200. D. desulfuricans G200(pJRC800F20L) cells (370 g, wet weight) were obtained from 300 L of fermentation in medium C supplemented with 0.26 mM kanamycin. Cells were harvested as previously described (*15*). The cells were suspended in 1100 mL of 50 mM Tris-HCl and 50 mM EDTA, pH 9.0; stirred for 30 min at 37 °C, and removed from the suspension by centrifugation (1 h at 27 000*g*). The supernatant, containing the periplasmic proteins, was further processed by column chromatography. The F20L cytochrome c_3 was isolated by a procedure essentially the same as for wild-type cytochrome (*15*). The two cytochromes c_3 present in extracts from *D. desulfuricans* G200(pJRC800F20L), namely the F20L cytochrome c_3 and the endogenous cytochrome c_3 from *D. desulfuricans* G200, were separated with a DEAE cellulose column as they have different isoelectric points, the latter being an acidic molecule and the former a basic one. The F20L cytochrome c_3 was found to be pure by electrophoresis on polyacrylamide gel under denaturing conditions (Phast System, Pharmacia) after two chromatographic steps using hydroxylapatite (Bio-Rad) and then CM-cellulose resins.

The concentration was determined spectrophotometrically (BECKMAN DU-7500) using an absorption coefficient ϵ of 115 000 M^{-1} cm^{-1} at 553 nm in the reduced state (*8*).

Hydrogenase Purification. The purification procedure was carried out at +4 °C with buffers saturated with argon in order to remove oxygen, except for the extraction step as described in ref 16. Hydrogenase activity was routinely determined at room temperature by the hydrogen consumption assay using methyl viologen as the electron acceptor and hydrogen as the electron donor. The hydrogen-dependent reduction rate of methyl viologen was followed spectrophotometrically at 604 nm (ϵ_{604} = 13600 M^{-1} cm^{-1}). The assay (1 mL in anaerobic cuvette) contained an oxygen consumption system (250 units/mL catalase, 0.5 units/mL glucose oxidase, 2.5 mM glucose), 1 mM methyl viologen, and 50 mM HEPES buffer, pH 7. It was flushed with argon (10 min) and then with hydrogen (10 min). At time zero, the reaction was started by adding the enzyme. One unit of enzyme activity is defined as the amount of enzyme required for the reduction of 1 μmol of methyl viologen/ min, with excess of hydrogen.

Isoelectric Point Measurements. The isoelectric point of the protein was determined by performing isoelectric focusing using a Phast System apparatus from Pharmacia LKB Biotechnology. Phast Gel IEF 3-9, which operates in the 3−9 pH, and ampholine polyacrylamide gel plates from Pharmacia (pH range 3.5−9.5) were used together with a Pharmacia broad-range pI calibration kit containing proteins with different isoelectric points ranging 3−10.

Molecular Mass Determination. Mass spectrometry analysis was carried out on a Perkin-Elmer Sciex API III triple quadripole mass spectrometer equipped with a nebulizer-assisted electrospray (ionspray) source. The spectra were recorded as described previously (*17*).

Analysis for Iron and Heme Content. The iron content was determined by plasma emission spectroscopy using a Jobin Yvon model JY 38 apparatus. The total number of heme units was determined using the pyridine ferrohemochromogene test. A known mass of the protein (determined by hydrolyzing an aliquot of protein solution and performing quantitative amino acid analysis) was added to an aqueous alkaline (0.0075 M NaOH/pyridine 25%) solution and reduced by adding a few crystals of sodium dithionite, the heme content was determined from the pyridine ferrohemochrome spectrum, using the millimolar absorbance coefficient of 29.1 at 550 nm with the cytochrome derivative (*18*).

Amino Acid Analysis and Protein Sequencing. For the amino acid analysis, protein samples were hydrolyzed in 200 μL of 6 M HCl at 110 °C for 24 and 72 h in sealed vacuum tubes and then analyzed with a Beckman amino acid analyzer (System 6300). Heme was removed using Ambler's method (*19*) and the resulting apoprotein was isolated by gel filtration on Sephadex G 25 in 5% (vol/vol) formic acid. Sequence determinations were carried out on the apoprotein with an Applied Biosystems gas-phase sequenator (models 470A and 473A). Quantitative determinations were performed on the phenyl thiohydantoin derivatives by means of high-pressure liquid chromatography (Waters Associates, Inc.) monitored by a data and chromatography control station (Waters 840). S-Carboxymethylated protein was prepared by dissolving the

apoprotein in 0.5 M Tris-HCl (pH 9.0), 8 M urea and 20 mM EDTA and treating it with iodoacetic acid, as previously described (*20*).

Kinetic Experiments. Anaerobic cuvettes were filled with the oxygen consumption system described above, in the presence of various concentrations of either wild-type or F20L cytochrome c_3 and 50 mM HEPES (pH 7). The absorbance at 553 nm was measured after the addition of 0.8 nM of hydrogenase. The slope of the tangent drawn at the beginning of the recorded trace was used to calculate the hydrogen oxidation rate. Theoretical curves were fitted to the experimental data with Sigma Plot software.

Scanning Microcalorimetry. Scanning microcalorimetric measurements were carried out on a DASM-4 differential scanning microcalorimeter (NPO Biopribor, Pushchino, Russia) in 0.48 mL cells at a heating rate of 1 K/min. An extra pressure of 2 atm was maintained during all DSC runs to prevent possible degassing of the solutions on heating. Protein solutions were prepared in 100 mM Tris-HCl buffer at pH 7.6 and extensively dialyzed before measurement against the same buffer at 4 °C during 24 h. Protein concentration varied from 1.5 to 2.9 mg/mL. No concentration dependence of the cytochrome denaturation parameters was observed in this concentration range. The heating curves were corrected for an instrumental baseline obtained by heating the solvent used for protein solution. The reversibility of the unfolding was checked routinely by sample reheating after cooling in the calorimetric cell. The partial molar heat capacity of the protein (C_p) was determined as described elsewhere (*21*), with the partial specific volume of 0.72 cm^3 g^{-1} calculated according to ref 22. The excess heat capacity curves used to determine the calorimetric heat effect (Q_{cal}) were obtained with the SCAL2 software package (*23*). The calorimetric heat effect values were accurate to ±6%, C_p values were accurate to ±0.3 kcal/K mol, and the denaturation temperatures were accurate to ±0.2 °C.

Circular Dichroism. CD spectra were recorded on a Jasco J-715 spectropolarimeter (Japan) equipped with thermostated water-jacketed cells (Hellma Cells) and a Neslab RTE-111 programmable circulating water bath (Neslab Instruments). The cells had a light path of 0.02 cm, protein concentration was 1.5−2.8 mg/mL. For continuous melting of the samples, the temperature was increased at 1 K/min. The results were expressed as molar circular dichroic absorption, $\Delta\epsilon$ (M^{-1} cm^{-1}), assuming that the molecular mass of holocytochrome c_3 is 14 087 Da. The $\Delta\epsilon$ was determined as $\Delta\epsilon = \theta/33cl$, where c is the molar protein concentration, l is the light path in centimeters, and θ is the measured ellipticity in degrees. The instrument was calibrated with Jasco standard nonhydroscopic ammonium (+)-10-camphorsulfonate, assuming molar ellipticity $[\Theta]_{290.5} = 7910$ deg cm^2 $dmol^{-1}$ (*24*). Noise in the data was smoothed using the Jasco J-715 software, including the fast Fourier transform noise reduction routine which allows enhancement of most noisy spectra without distorting their peak shapes.

Crystallization and 3-D Structure Determination. The crystals were grown by the vapor diffusion method (*25*) using the hanging drop variant. Drops composed of 3 μL of protein solution (13 mg/mL in 40 mM Tris-HCl pH 7.6) and 3 μL of precipitant solution were equilibrated at 20 °C against reservoirs containing 500 μL of the same precipitant solution, which consisted of 3.3−3.4 M $(NH_4)_2SO_4$ solution and 100 mM Tris-HCl buffer (pH 9). The crystals take several weeks to appear and 2−3 months to reach a suitable size (0.2 × 0.2 × 0.2 mm^3) for X-ray diffraction analysis. The crystals were found to be tetragonal, space group *P*4 with cell dimensions $a = b = 97.22$ Å and $c = 36.03$ Å, and eight molecules in the cell, thus corresponding to two molecules in the asymmetric unit.

Table 2: Data Collection, Molecular Replacement, and Refinement Parameters for F20L c_3

space group	P4
cell dimensions (Å)	$a = b = 97.22$ $c = 36.03$
resolution range (Å)	23−2.3 (2.35−2.30)
total number of observations	48 916
no. of unique observations	14 381 (946)
percent of data	92.3 (93.2)
R_{sym} (%)	6.3 (50.5)
$I/\sigma I$	16.4 (2.4)
correlation coefficient and *R*-factor of MR solutions	(resolution range 10−3.5 Å)
Mol A/Mol B (%)	25.1; 49.0/22.1; 50.8
Mol A + B (%)	35.1; 45.1
no. of non hydrogen atoms	1874
no. of solvent sites	107
missing residues	1A−7A; 1B−19B
R-factor (%)/no. of reflections	22.4/12450
R_{free} factor (%)/no. of reflections	29.6/1367
rms deviations in	
bond lengths (Å)	0.014
bond angles (deg)	1.78
ramachandran outliers	Cys51

X-ray intensity data were collected from a single-crystal mounted in a glass capillary, on the EMBL X31 beam line at the DORIS storage ring, DESY, Hamburg, with a wavelength of $\lambda = 1.07$ Å. The intensities were measured using a MARresearch imaging plate bi-dimensional detector and processed with the DENZO program package (*26*, *27*). Data were collected up to a maximal resolution of 2.3 Å. The statistics on the diffraction data are summarized in Table 2. The correct orientation of the protein molecule within the new unit cell was found by molecular replacement using the program AMoRe (*28*). The cross-rotation calculations were performed using as model the published coordinates (pdb code 1cth) of the native cytochrome c_3 from *D. vulgaris* Hildenborough (*29*). Two independent solutions, corresponding to the two molecules in the asymmetric unit, were found and the correlation coefficients and *R*-factors are listed in Table 2. The structural refinement was carried out with the XPLOR3.8 program package (*30*). ($2F_o - F_c$) maps and ($F_o - F_c$) maps were calculated and inspected after each round of refinement and the structural changes were constructed with the graphical program TURBO-FRODO (*31*).

Two independent molecules A and B were modeled. NCS restraints were only applied in the first two refinement cycles. Ten percent of the reflections were set aside for cross validation analysis (*32*) and used to monitor the various refinement strategies such as geometric and temperature-factor values and the insertion of the solvent water molecules. All data from 23 to 2.3 Å resolution were employed in the refinement and therefore a low resolution bulk solvent correction was applied, as implemented in X-PLOR3.8 (*30*). Coordinates for the structure described in this work have been deposited with the Brookhaven Protein Data Bank (ref 33; pdb code 1mdv).

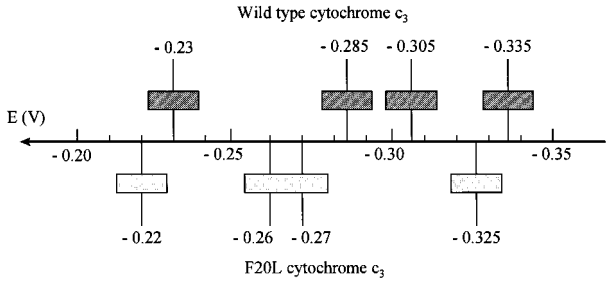

FIGURE 1: Macroscopic redox potentials values of the heme groups in both wild-type and F20L cytochromes c_3. Values are accurate to ±10 mV.

RESULTS

Isolation of F20L Cytochrome c_3. F20L cytochrome c_3 was found to be pure with a purity coefficient (A553 red − A570 red/A280 ox) of 3.0. The yield was about 170 mg of pure protein (0.56 mg/g of cells) which is three times higher as that obtained for the wild-type protein expressed in *D. desulfuricans* (0.2 mg/g cells) (*15*). The UV−vis spectra showed no difference from that of the wild-type cytochrome c_3. The amino acid composition is in complete agreement with the amino acid composition derived from the sequence. F20L cytochrome c_3 has the same isoelectric point (10.5) as the wild-type protein. Its NH_2 terminal sequence (up to residue 24) was found to be identical to that of the native protein, except at position 20 where a leucine residue was detected instead of a phenylalanine, indicating that the polypeptide is successfully matured in *D. desulfuricans* G200 during transport to the periplasm.

Native electrophoresis was performed with both wild-type and F20L cytochromes c_3 preincubated at various temperatures (30, 60, and 100 °C). The electrophoretic pattern showed no differences between the two proteins, indicating that the mutation does not induce a polymerization of the molecule (data not shown). The reconstructed mass spectra of F20L cytochrome gave only one peak corresponding to the molecular mass of 14 085 ± 2 Da, which is consistent with the calculated molecular mass of 14 087 Da with the phenylalanine/leucine replacement.

The four macroscopic redox potentials of F20L cytochrome c_3 were determined by electrochemistry using the equipment and theoretical analysis described before (*8*). The measured values are compared to those of the wild-type cytochrome in Figure 1. It appears that the F20L replacement induces significant changes on the four macroscopic redox potentials of the molecule, which vary by up to 30 mV.

Electron Transfer between [Fe] Hydrogenase and F20L Cytochrome c_3. To analyze the effect of the mutation on the electron-transfer properties of the cytochrome, we have studied the kinetics of reduction of F20L cytochrome c_3 by the [Fe] hydrogenase. In our conditions, the hydrogenase was in a reduced state, and this state can be considered constant during the reaction due to the excess of molecular hydrogen (over 20 times the K_m value). The steady-state rate of reduction of F20L cytochrome followed Michaelis−Menten kinetics (Figure 2A), and the corresponding Hill coefficient is equal to 1.02 ± 0.02. These results suggest a lack of intermolecular cooperativity between the redox centers and are different from those obtained when the wild-type cytochrome c_3 was used (*16*) (Figure 2B). With the latter,

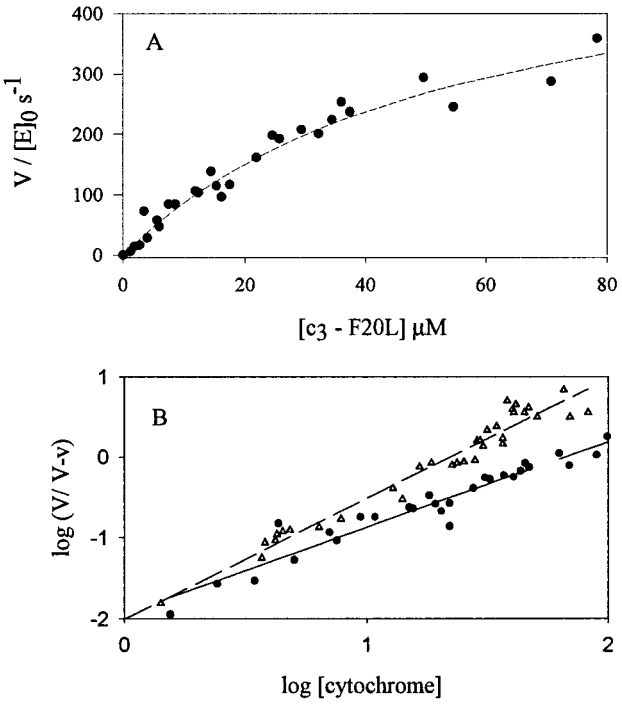

FIGURE 2: Kinetic behavior of cytochrome c_3 reduction by [Fe] hydrogenase. (A) Kinetic behavior of the reaction between F20L cytochrome c_3 and [Fe] hydrogenase. The curve was fitted to Michaelis−Menten equation. The values of the deduced kinetic parameters were $V_m = 533 \pm 37$ s^{-1} and $K_m = 40 \pm 6$ μM. (B) Hill plot pertaining to the region of maximun slope of cytochrome reduction. (●) F20L cytochrome c_3; (△) wild-type cytochrome c_3. The corresponding Hill coefficients are 1.02 ± 0.02 and 1.37 ± 0.02, respectively.

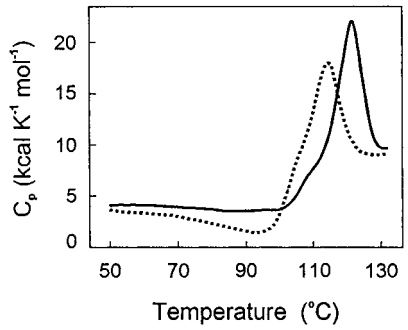

FIGURE 3: Temperature dependence of the partial molar heat capacity of cytochrome c_3 (solid line) and its F20L mutant (dotted line) at pH 7.6.

the Hill coefficient is equal to 1.37 ± 0.1, the electron transfer appearing thus to be a positive cooperative process. The kinetic parameters deduced from our data were found to be 533 ± 37 s^{-1} for the catalytic constant and 40 ± 6 μM for the Michaelis−Menten constant.

Scanning Calorimetry. Figure 3 shows the temperature dependence of the partial heat capacity for wild-type cytochrome c_3 and its F20L mutant up to 131.8 °C, the high-temperature limit of our microcalorimeter. The partial molar heat capacities at 20 °C (C_p^{20}) of cytochrome c_3 is equal to 3.8 kcal/K mol. This value calculated per gram of protein, 0.27 cal/K g, is lower than the average value of the partial specific heat capacity at 20 °C for small globular proteins, 0.31 cal/K g (*34*). It might be considered an indication that cytochrome c_3 is less flexible than other small proteins. There is a structural basis for this since the core part of cytochrome

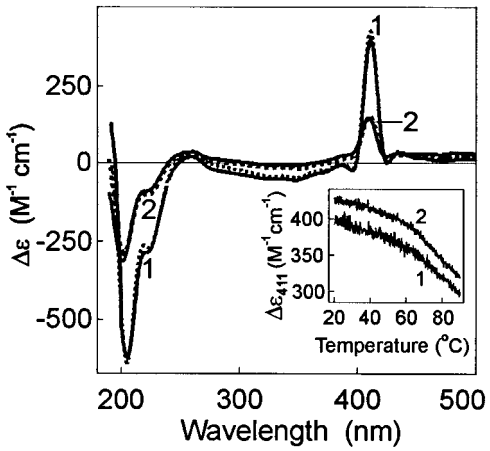

FIGURE 4: CD spectra of cytochrome c_3 (solid line) and its F20L mutant (dotted line), in the 190−500 nm region at pH 7.6: (1) 20 °C and (2) after heating in the calorimetric cell to 130 °C and then cooling to 20 °C. (Inset) Temperature dependence of the Soret band intensity decrease of cytochrome c_3 (1) and its F20L mutant (2).

c_3, held together by eight covalent links between the cysteine residues and the heme-vinyl groups, is a very rigid feature and must be less flexible than the core of other small proteins of comparable size. Contrary to other globular proteins (*34*), and also to cytochromes c_7 and cytochrome *c* (M_r 50 000) from *Desulfuromonas acetoxidans* (unpublished data), for which the C_p value increases linearly with temperature until the denaturation temperature range is reached, for both wild-type and F20L cytochromes c_3, the C_p increases in the temperature interval 5−25 °C and does not change up to 50−55 °C (data not shown). The partial heat capacity decreases with subsequent temperature increase until the beginning of heat absorption connected with protein denaturation (Figure 3). This type of behavior points to the existence of some exothermal process resulting from a slight nonspecific self-association caused by heating which is stronger for F20L cytochrome. The reproducible shoulder in the left part of calorimetric peaks can reflect the disruption of this interaction at the early stage of denaturation. The heat denaturation of both wild-type and F20L cytochromes c_3 is irreversible. However, scanning calorimetry shows no sign of detectable aggregation after denaturation and the shape of calorimetric peaks was not disturbed while changing the cytochrome concentration in the range 1.5−2.9 mg/mL.

Both wild-type and F20L cytochromes c_3 are extremely thermostable with the respective denaturation temperatures of 121.6 and 114.3 °C. Thus, the F20L substitution leads to the decrease in cytochrome c_3 thermostability by 7.3 °C. The values of calorimetric heat effect for wild-type and F20L cytochromes are very close.

Circular Dichroism in the 190−500 nm Region. As it is known, CD spectra in peptide bond and Soret absorption regions correspond to different structural properties of macromolecules. Whereas circular dichroism in Soret region represents the asymmetric environment of the heme groups, CD in far-UV region reflects a macrostate of the protein which depends on the overall secondary peptide chain structure (*35*). Figure 4 (curves 1) shows the CD spectra of wild-type cytochrome c_3 and its F20L derivative at 20 °C. As CD spectra are almost identical, the mutation does not change the native secondary structure of the protein and the state of hemes local surroundings. Earlier, we have found that point mutations in cytochrome c_3—H22M, H25M, H35M, and H70M—do not change the secondary structure and the local structure of the hemes vicinity (*9*), and in ref *7* authors have shown that F20I cytochrome c_3 maintains the same overall structure near the heme groups and the structural arrangement of the four-heme core.

The inset of Figure 4 demonstrates that at very long before the temperature of heat denaturation there is an essential, noncooperative decrease of CD value in the Soret region with temperature for both cytochromes. The same is valid for the far-UV region (205 nm). These temperature dependencies consist of two parts with different slopes and the inflection region practically coincides with the temperature at which the heat capacity of cytochromes begin to decrease (Figure 3). Note that protein concentration used in calorimetry and CD was the same. This means that the temperature alteration in the asymmetric environment of the prosthetic groups and some secondary structure alteration takes place before the thermal cooperative transition. In our previous paper (*9*), small CD intensity fall for cytochrome c_3 produced by temperature (50−97 °C) in Soret region was also observed, but there was no change in the CD amplitude at 205 nm, which, possibly, is explained by the significantly less protein concentration (0.3 mg/mL) used comparing with the present study (1.5−2.8 mg/mL). The effect of an essential, noncooperative decrease of CD value with temperature for both cytochromes supports our supposition drawn from the calorimetric data on the existence of nonspecific self-association caused by heating.

Despite the irreversibility of cytochromes denaturation, observed by microcalorimetry, CD spectra of both wild-type and F20L cytochromes c_3, obtained after the denaturation and cooling from 130 to 20 °C, retain sufficiently large intensities in the Soret region, (Figure 4, curve 2). Hence, the anisotropy of hemes core microenvironment is not fully destroyed even after denaturation at extremely high temperatures. This fact testifies that the structure of cytochrome c_3 heme core is uniquely stable. When the heme region is disturbed, as in a set of cytochrome c_3 mutants in which the histidine, sixth axial ligand of each iron atom, was replaced by a methionine residue (*9*), CD in the Soret region completely disappears after denaturation.

3D Structure Determination. A summary of data quality and completeness is given in Table 2. The mutant cytochrome c_3 F20L data consist of 48 916 observations of 14 381 unique reflections. The electron density maps were of good quality and allowed to correct for changes with respect to the native protein structure (Figure 5). The final model consists of two NCS-related molecules A and B and 107 water molecules; for molecule A, residues 8−107 were visible, while for molecule B, only poor density was visible for the residues 8−20 and these residues were therefore modeled as in molecule A and given an occupation factor of 0.3 to indicate that the modeled structure is one of several possible conformations. Furthermore, some of the side-chain atoms of several lysine residues (29a; 40a,b; 45a,b; 58a,b; 63a,b; 72a,b; 75a,b; 77a,b; 93a,b; 94b; 95a,b; 102a,b; 104a,b) and some other residues (36−38a and 37b, 38b, 41b and 42b) on the surface of the molecule have been given occupations of 0.3, to simulate the local disorder of these residues. The molecule has a particularly high overall *B*-factor of 38.53 Å^2, as derived from intensity statistics (*36*).

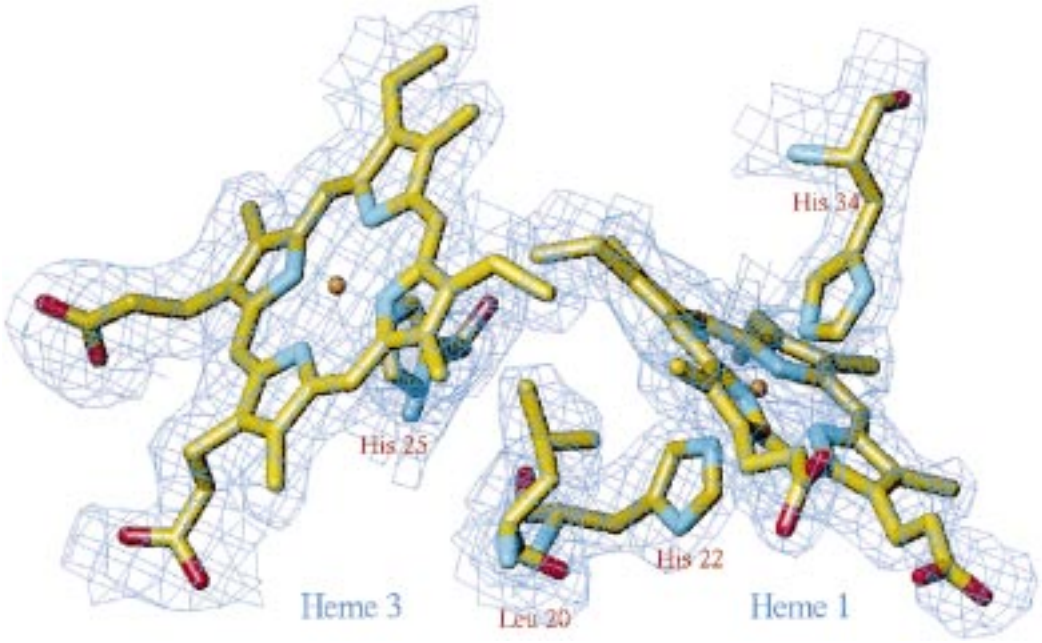

FIGURE 5: The final $2F_o - F_c$-map surrounding hemes 3 and 1 and the mutated site Leu20. The electron density is shown at a level of 1σ. This figure, as well as Figures 6 and 7, are produced with the program TURBO-FRODO (*31*).

The average *B*-factor for the two modeled protein molecules (excluding the water molecules) at the end of refinement is 43.58 Å^2. This rather high thermal motion could be one of the explanations for the high number of disordered residues on the surface of the molecule. The final model structure has an *R*-factor of 0.22 with an R_{free} (*32*) of 0.29. All the nonglycine residues have conformational angles (Φ,Ψ) in permitted regions of the Ramachandran plot, except Cys51, which has a particular conformation in all cytochrome c_3 structures (*4*, *37*−*39*). The heme numbering scheme, adopted in this paper, corresponds to the order of appearance in the primary sequence of the cysteines that covalently link the heme groups.

The overall structural fold is substantially the same as in the native structure (Figure 6) and the 4 heme-core superposes with an rmsd of 0.23 Å. Two regions, however, deviate by more than 1 Å from the native structure: the N-terminal residues 8−20, as far as modeled, up to the site of mutation, and the C-terminal region, including residues 104−107. The N-terminal region includes the only short two-stranded antiparallel β-sheet, present in all tetraheme cytochromes c_3, and loop 1 (see ref 4 for the description of the loops). The C-terminal region contains one helical loop of the heme-binding sequence C−X−X−X−X−C−H of heme 4. Both regions have undergone a substantial structural rearrangement and are involved in intermolecular contacts between molecules A and B, related by the noncrystallographic 2-fold axis (see Table 3). The two NCS-related molecules form a type of crystallographic dimer with several residues forming hydrogen bridges across the interface. This interface covers a surface of 1097.9 Å^2, which can be considered as that of a typical dimeric protein (*40*). Furthermore, the 2-fold axis brings the hemes 4 of molecules A and B close to each other and a heme stacking similar to that observed in the dimeric cytochrome c_3 (M_r 26 000) (*4*) is obtained (distance Fe heme 4 Mol A−Fe heme 4 Mol B = 9.71 Å). In the mutant structure, the N-terminal region seems completely disordered, the β-sheet does not exist anymore, and the loop 1 is turned by 20° out, to avoid to bump into the residues of same region of the second molecule in the asymmetric unit. Therefore, the question arises, if this structural rearrangement is due to the crystal packing contacts or due to the mutation.

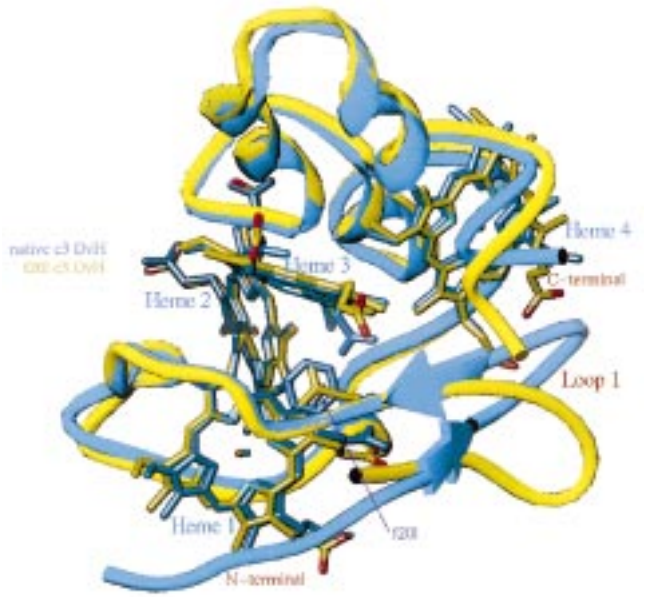

FIGURE 6: Ribbon representation of the superposition of the wild-type (yellow) and F20L (blue) cytochromes c_3 structures. Marked changes are seen for the N-terminal and C-terminal regions.

Two different native crystal forms have been reported for *D. vulgaris* Hildenborough cytochrome c_3 and the 3-D structures are determined (*29*, *38*). Both show an identical conformation at the N-terminal, comprising the short β-sheet and loop 1, indicating that no particular flexibility has been observed for this loop. Furthermore, the highly homologous cytochrome c_3 from the Miyazaki strain is also perfectly superposable in the region between residues 2 to 21 (*37*). In other cytochromes c_3, the loop 1 site varies by the length of the loop; the two-stranded β-sheet, however, superposes

Table 3: Crystal-Packing Contacts (Å) between Symmetry−Related Molecules (Crystallographic sym0−sym1 with Neighboring "octamer", sym0−sym3 around the 4-fold Axis and Noncrystallographic MolA−MolB

	interatomic distance		interatomic distance
atoms sym0−sym1		atoms sym0−sym3	
D59A $O^{\delta1}$-D59B $O^{\delta2}$	2.75	Hem1 Cma−Hem1 O1a	3.27
K58A O−K60B N	3.30	Hem1Cbb−Hem1 Chb	3.63
K60A N−K58B O	3.11	atoms MolA−MolB	
atoms sym0−sym3		K15A O−Q16B Ne^2	2.99
D7A $O^{\delta2}$−E41B O	2.90	Q16A $N^{\epsilon2}$−K15B O	3.96
D7A N−Y43B O	3.12	K15A O−Hem4 O2a	3.60
K26A N^{ζ}−E41B $O^{\epsilon2}$	3.73	K57A N^{ζ}−K101B O	3.54
K26A N^{ζ}−Y43B O^{η}	3.23	K58A N^{ζ}−E107 $O^{\epsilon2}$	3.66
G39A O−N38B $N^{\delta2}$	3.09	Hem4 Caa−Hem4 Caa	3.68
E41A N−N38B $O^{\delta1}$	3.70	Hem4 C3a−Hem4 C3a	3.97
Y43A O^{η}−G8B O	3.46	Hem4 O2d−Hem4 O1a	3.35

perfectly well in all these structures (*4*). Phe20 is situated in the heart of the heme core, the ring plane being almost parallel to the plane of heme 1 and perpendicular to that of heme 3. Together with the histidine residues, axial ligands to the heme iron atoms, Phe20 forms a tight hydrophobic packing with a minimum of cavities at the heart of the 4-heme core. Phe20 seems to be the central residue in this hydrophobic packing. Close hydrophobic packing is known to be important for the stabilization of protein folds (*41*−*43*). One can notice in Figure 6, that the side chain atom Cγ of Leu20 is centered in the middle of the aromatic ring of Phe20. To obtain this position, the whole residue, including the main-chain atoms of Leu 20, is shifted by about 0.9 Å inside the hole, created by the missing atoms of the aromatic ring. This induces a change in the (Φ,Ψ) angles of Leu20, and the preceding residues and the formation of the β-sheet is no longer possible. The main secondary structure element of the N-terminal residues is missing and therefore they are disordered.

The crystal packing can be described as a tetramer of the dimers related by the NCS-2-fold axis (Figure 7), leading to octamers around the crystallographic 4-fold axis. No such close intermolecular contacts have been reported for either of the two native structures determined in two different crystallographic systems (*29*, *38*). In the hexagonal form there are also two molecules in the asymmetric unit, but they are related by a translation rather than a rotation axis and no intermolecular contacts such as in the mutant crystal form have been observed. It seems, as if the mutation destabilizes the secondary structure of the N-terminal region (1−19), and because of the disorder of the N-terminal end, the close contacts, found in the crystallographic dimer, are possible.

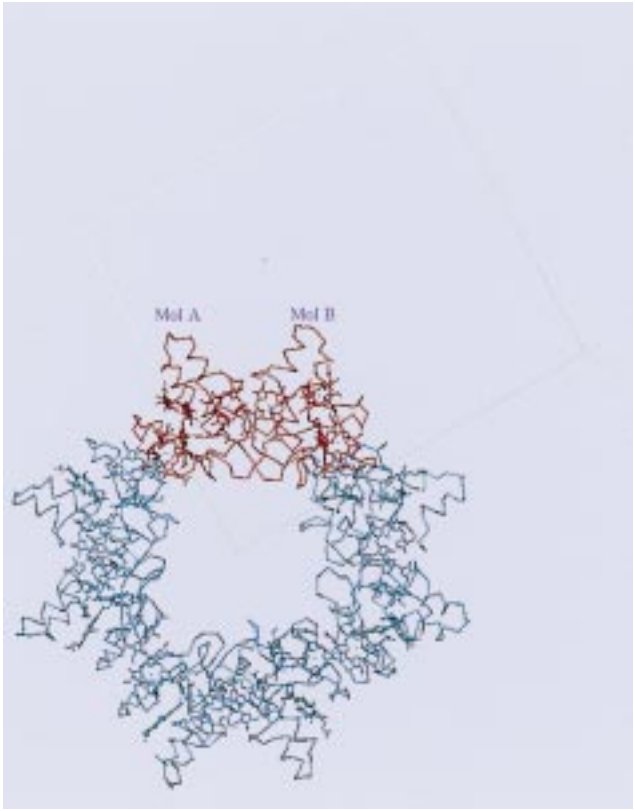

FIGURE 7: Crystal packing of the F20L cytochrome c_3. The two molecules in the asymmetric unit, Mol A and Mol B, are shown in red and the symmetry related molecules around the 4-fold crystallographic axis are shown in blue.

DISCUSSION

A recent report (*7*) on substitutions of Phe20 in cytochrome c_3 from *D. vulgaris* Hildenborough by serine, tryptophane, tyrosine, and isoleucine showed that only the later two were expressed normally, and it was assumed that the serine and tryptophan mutants are not properly folded. The F20Y derivative was expressed with a very low yield and it was assumed that it is less stable. Only the F20I mutant appeared to be correctly expressed and the yield obtained was almost the same as that obtained for the wild-type protein, produced in *D. desulfuricans* (0.16 mg/g of cells) (*7*). In the same study, Saraiva et al. reported that the EPR and NMR study of F20I revealed only small changes due to the mutation, which probably caused some structural changes but had no influence on electron/electron or proton/electron cooperativity. In the case of the F20L cytochrome c_3 that we analyzed, the three times higher yield (0.56 mg/g of cells) may be due to the purification procedure after periplasmic extraction, it could also be due to a better expression of the recombinant protein. The differences in yield of protein when the Phe20 residue is replaced by various amino acids suggest that this residue position might have a key role in the folding of the molecule.

Even if F20L cytochrome c_3 is still extremely thermostable with a denaturation temperature of 114.3 °C, the amino acid substitution at position 20 induced a decrease in the molecule thermostability of 7.3 °C. This decrease highlights the importance of the nature of the residue at position 20 in cytochrome c_3 in maintaining the thermostability property of the molecule.

In contrary to the sixth axial ligand to the heme iron replacement that we have already studied (*9*), the F20L replacement does not induce a perturbation of the heme region. On the other hand, the four macroscopic redox potentials are affected by the mutation. Surprisingly, Saraiva et al. (*7*) reported that only one macroscopic redox potential was changed when F20 was replaced by either tyrosine or isoleucine. The macroscopic redox potentials values are thus very sensitive to the nature of the amino acid in position 20. A small difference, such as Ile *versus* Leu, might induce strong effects.

The parameters of the reduction of the F20L cytochrome by the [Fe] hydrogenase as deduced from the kinetic experiments are not really different from those obtained when wild-type cytochrome c_3 is used (*16*). The Michaelis−Menten constants are in the same range, 40 ± 6 and 33 ± 8 for F20L and wild-type cytochromes, respectively. This fact suggests that the mutation has no effect on the interaction between the cytochrome and the hydrogenase. In the same way, there is no high difference between the catalytic constant.

On the other hand, our present study shows an important effect of the mutation on the process of reduction of F20L cytochrome by the [Fe] hydrogenase. In the wild-type cytochrome, the electron transfer between the two molecules appears to be a cooperative phenomenon ($h = 1.37$). This cooperative behavior could be related to the conductivity properties of the cytochrome molecules, which have already been measured for multihemic cytochromes (*44*). Surprisingly, this intermolecular cooperativity between the cytochrome molecules is lost in the F20L cytochrome, as the value of the Hill coefficient suggests ($h = 1.02$). On the basis of the known structure of cytochrome c_3 (*29*) and of the hypothesis of the intramolecular electron-transfer pathway, heme 4 being the entrance gate, passing by heme 3 and then to heme 1 (*6*), we proposed that one molecule of cytochrome c_3 interacts with an other one so that heme 1 of the first molecule is in close contact with heme 4 of the second cytochrome molecule (*16*). The structural changes observed in the F20L cytochrome concerns the N-terminal region, which surrounds heme 1 in the wild-type structure. The introduced structural flexibility of the N-terminal region in the F20L cytochrome could explain the lack of cooperativity, in the way that the unstructured N-terminal polypeptide chain could sterically hinder a correct interaction of heme 1 with heme 4 of an other molecule, or simply does not contain anymore the structural conformation required for an effective interaction. The key role of F20 in the intramolecular electron exchange might also be an explanation, the intramolecular electron exchange between heme 3 and heme 1 being drastically affected by the F20L replacement. Analysis of the intramolecular electron exchanges between the four hemes of both wild-type and F20L cytochromes c_3 will be the following step of this study.

ACKNOWLEDGMENT

We gratefully acknowledge the contribution of G. Leroy for site directed mutagenesis and protein purification, J. Wall for the transconjugaison, R. Toci (Fermentation Plant Unit L.C.B., Marseille France) for growing the bacteria, P. Bianco for redox potential determination, and N. Zylber and J. Bonicel (Protein sequencing Unit, B.I.P., Marseille, France) for performing the amino acid analysis and N-terminal sequence determination. We also thank Dr. J. C. Germanique for the iron content analysis and Dr. Forest for mass determination.

REFERENCES

1. Ambler, R. P. (1980) in *From cyclotrons to cytochromes* (Robinson, A. B., and Kaplan, N. O., Eds.) pp 263−279, Academic Press, London.
2. Bruschi, M., Loutfi, M., Bianco, P., and Haladjain, J. (1984) *Biochem. Biophys. Res. Commun. 120*, 384−389.
3. Odom, J. M., and Peck, H. D. (1984) *Annu. Rev. Microbiol. 38*, 551−592.
4. Czjzek, M., Guerlesquin, F., Bruschi, M., and Haser, R. (1996) *Structure 4*, 395−404.
5. Matias, P. M., Morais, J., Coelho, R., Carrondo, M. A., Wilson, K., Danter, Z., and Sicker, L. (1996) *Protein Sci. 5*, 1342−1354
6. Dolla, A., Guerlesquin, F., Bruschi, M., and Haser, R. (1991) *J. Mol. Recognit. 4*, 27−33.
7. Saraiva, L. A., Salguiero, C. A., LeGall, J., VanDongen, W. M. A. H., and Xavier, A. V. (1996) *J. Biol. Inorg. Chem. 1*, 542−550.
8. Mus-Veteau, I., Dolla, A., Guerlesquin, F., Payan, F., Czjzek, M., Haser, R., Bianco, P., Haladjian, J., Rapp-Giles, B. J., Wall, J. D., Voordouw, G., and Bruschi, M. (1992) *J. Biol. Chem. 267*, 16851−16858.
9. Dolla, A., Florens, L., Bruschi, M., Dudich, I. V., and Makarov, A. A. (1995) *Biochem. Biophys. Res. Commun. 211*, 742−747.
10. Maniatis, T., Fritsch, E. F., and Sambrook, J. (1982) *Molecular Cloning, a Laboratory Manual*, Cold Spring Harbor Laboratory, Plainview, NY.
11. Postgate, J. R. (1984) *The Sulphate-Reducing Bacteria*, 2nd ed., Cambridge University Press, Cambridge.
12. Voordouw, G., and Brenner, S. (1986) *Eur. J. Biochem*. 159, 347−351.
13. Taylor, J. W., Ott, J., and Eckstein, F. (1985) *Nucleic Acids Res. 13*, 8764−8785.
14. Sanger, F., Nicklen, S., and Coulson, A. R. (1977) *Proc. Natl. Acad. Sci. U.S.A. 87*, 5463−5467.
15. Voordouw, G., Pollock, W. B. R., Bruschi, M., Guerlesquin, F., Rapp-Giles, B. J., and Wall, J. M. (1990) *J. Bacteriol. 172*, 6122−6126.
16. Brugna M., Giudici-Orticoni M. T., Spinelli S., Brown K., Tegoni M., and Bruschi M. (1998) *Proteins* (in press).
17. Bruschi M., Woudstra M., Guigliarelli B., Asso M., Lojou E., Petillot Y., and Abergel C. (1997) *Biochemistry 36*, 10601−10608.
18. Falk J. E. (1964) *Porphyrins and Metalloporphyrins*; *Their general Physical and Coordination Chemistry and Laboratory Methods*, p 240, Elsevier, New York.
19. Ambler R. P. (1963) *Biochem. J.* 89, 338−349.
20. Crestfield, A. M., Moore, S., and Stein, W. H. (1963) *J. Biol. Chem. 238*, 622−627.
21. Privalov, P. L., and Potekhin, S. A. (1986) *Methods Enzymol. 131*, 4−51.
22. Makhatadze, G. I., Medvedkin V. N., and Privalov, P. L. (1990) *Biopolymers 30*, 1001−1010.
23. Filimonov, V. V., Prieto, J., Martinez, J. C., Bruix, M., Mateo, P. L., and Serrano, L. (1993) *Biochemistry 32*, 12906−12921.
24. Takakuwa, T., Konno, T., and Meguro, H. (1985) *Anal. Sci. 1*, 215−225.
25. McPherson, A. (1982) *Preparation and Analysis of Protein Crystals*, Wiley, New York.
26. Otwinowski, Z. (1993) In *Proceedings of the CCP4 Study Weekend: Data Collection and Processing* (Sawyer, L., Isaacs, N., and Bailey, S., Eds.) pp 56−62, SERC Daresbury Laboratory, Warrington, U.K.
27. Minor, W. (1993) *XDISPLAYF program*, Perdue University, West Lafayette, IN.

28. Navaza, J. (1994) *Acta Crystallogr., Sect A 50*, 157−163.
29. Matias, P. M., Frazao, C., Morais, J., Coll, M., and Carrondo, M. A. (1993) *J. Mol. Biol. 234*, 680−699.
30. Brünger A. T. (1996) *X-PLOR program*, Version 3.8, Yale University, New Haven, CT.
31. Roussel, A., and Cambillau, C. (1992) *TURBO−FRODO program, the manual*, Biographics, AFMB, Marseille, France.
32. Brünger, A. T. (1992) *Nature 355*, 472−475.
33. Bernstein, F. C., Koetzle, T. F., Williams, G. J. B., Meyer, E. T., Jr., Brice, M. D., Rodgers, J. R., Kennard, O., Shimanouchi, T., and Tasumi, M. (1977) *J. Mol. Biol. 112*, 535−542.
34. Privalov, P. L., Tiktopulo E. I., Venyaminov, S. Y., Griko, Y. V., Makhatadze, G. I., and Khechinashvili, N. N. (1989) *J. Mol. Biol. 205*, 737−750.
35. Myer, Y. P., and Pande, A. (1978) in *The Porphyrins* (Dolphin, D., Ed.) pp 271−322, Academic Press, New York.
36. Wilson, A. J. C. (1949) *Acta Crystallogr. 2*, 397−398.
37. Higuchi, Y., Kusunoki, M., Matsuura, Y., Yasuoka, N., and Kakudo, M. (1984) *J. Mol. Biol. 172*, 109−139.
38. Morimoto, Y. Tani, T., Okumura, H., Higuchi, Y., and Yasuoka, N. (1991) *J. Biochem. 110*, 532−540.
39. Czjzek, M. Payan, F., Guerlesquin, F., Bruschi, M., and Haser, R. (1994) *J. Mol. Biol. 243*, 653−667.
40. Janin, J. (1997) *Nat. Struct. Biol. 4*, 973−974.
41. Vogt, G., Woell, S., and Argos, P. (1997) *J. Mol. Biol. 269*, 631−643.
42. Richards, F. M. (1997) *Cell. Mol. Life Sci. 53*, 790−802.
43. Eriksson, A. E., Baase, W. A., Zhang, X.-J., Heinz, D. W., Blaber, M., Baldwin, E. P., and Matthews, B. W. (1992) *Science 255*, 178−183.
44. Kimura, K., Nakahara, Y., Yagi, T., and Inokuchi, H. J. (1979) *J. Chem. Phys. 70*, 3317−3323,

BI981593H